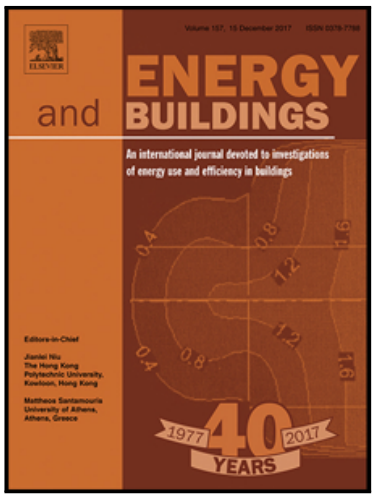

A novel comprehensive workflow for modelling outdoor thermal comfort and energy demand in urban canyons: results and critical issues

Gianpiero Evola , Vincenzo Costanzo , Cristina Magrì , Giuseppe Margani , Luigi Marletta , Emanuele Naboni

PII: S0378-7788(20)30077-3
DOI: https://doi.org/10.1016/j.enbuild.2020.109946
Reference: ENB 109946

To appear in: *Energy & Buildings*

Received date: 9 January 2020
Revised date: 26 February 2020
Accepted date: 11 March 2020

Please cite this article as: Gianpiero Evola , Vincenzo Costanzo , Cristina Magrì , Giuseppe Margani , Luigi Marletta , Emanuele Naboni , A novel comprehensive workflow for modelling outdoor thermal comfort and energy demand in urban canyons: results and critical issues, *Energy & Buildings* (2020), doi: https://doi.org/10.1016/j.enbuild.2020.109946

A novel comprehensive workflow for modelling outdoor thermal comfort and energy demand in urban canyons: results and critical issues

Gianpiero Evola[1], Vincenzo Costanzo[1], Cristina Magrì[2],
Giuseppe Margani[2], Luigi Marletta[1], Emanuele Naboni[3]

[1] *DIEEI, University of Catania, Viale A. Doria 6, 95125 Catania (Italy)*
[2] *DICAR, University of Catania, Via Santa Sofia 64, 95123 Catania (Italy)*
[3]*KADK, Philip de Langes Allé 10, 1425 Copenhagen, Denmark*

Abstract

In the energy simulation of buildings there has been little focus on their impact on the microclimate; simulation tools have usually dealt either with building or with outdoor simulation, and only recently these aspects are being interconnected. Within this framework, the paper describes a novel simulation workflow developed in the Grasshopper environment, where the Ladybug Tools are used to model the mutual relations amongst urban microclimate, building energy performance and outdoor thermal comfort. With reference to an urban canyon located in Catania, Southern Italy, the workflow – by coupling the indoor and the outdoor thermal field – provides both the dynamic thermal load of the buildings overlooking the canyon and the parameters needed to measure the outdoor comfort perceived by pedestrians. In comparison to other existing approaches, this workflow offers significant flexibility and makes it possible to perform a parametric investigation of the effects of different design solutions on both the indoor and the outdoor environment.

The outdoor Mean Radiant Temperature calculated through the model is compared to on-site measurements performed with a black globe thermometer during two different days in the summer. The comparison suggests good agreement in the shaded areas of the canyon, but a non-negligible overestimation in sunlit areas. These results have driven the authors to a critical insight into the algorithms implanted in the Ladybug Tools, and have helped to highlight some critical issues that will be further investigated in upcoming research.

Keywords: Mean Radiant Temperature, Universal Thermal Climate Index, Outdoor Comfort, Urban Heat Island, Urban Modelling, Grasshopper tools

1. Introduction

The energy demand for space heating and cooling is significantly influenced by the thermal properties of the building envelope. For this reason, national and international regulations have introduced strict requirements regarding the parameters that describe the steady and dynamic behaviour of the envelope components for new and refurbished buildings. On the contrary, there has been little focus on their impact on the local microclimate. The scope of codes and standards has been limited to maintaining indoor thermal neutrality, and has disregarded any of the thermal effects on surroundings.

Several works in the literature have recently pointed out non-negligible interactions between the outer envelope of buildings and the thermal field perceived outdoors by pedestrians [1]. Indeed, while outdoor microclimate influences the energy demand of buildings, it is also true that the building envelope influences the outdoor microclimate. In the past, common sense and tacit knowledge led to cities where outdoor spaces and buildings were finely integrated, and this contributed to comfortable outdoor and indoor climate achieved with little or no expenditure of energy. Then, the introduction of mechanical systems reinforced the idea that any building could be artificially acclimatised, and their overuse led to substantial rates of overheating also in the streets [2]. This occurs primarily in the so-called *urban canyons*: here, the morphology of the built environment modifies the distribution of the solar radiation received by the surfaces of the buildings, and locally reduces the wind speed, which in turn alters the rate of heat flow exchanged by convection between the facades and the outdoor air. These effects are exacerbated in the summer, often leading to pronounced outdoor thermal discomfort for pedestrians [3].

The geometry of a street canyon is typically defined through the height-to-width ratio H/W (also known as *aspect ratio*), where H is the average building height and W is the distance between the opposite sides of the canyon. In tall and narrow (deep) canyons, the access of solar radiation is restricted mainly in the winter, when the solar altitude angle is low; consequently, in the daytime, the dry-bulb air temperature keeps lower than in larger canyons, i.e. those with lower H/W ratio [3-4]. On the other hand, in the nighttime deep canyons hinder the radiative heat transfer to the sky vault, and determine higher air temperatures than in open spaces [1]. In the summer, deep canyons are less effective and allow the access of solar radiation more easily than in the winter, due to the high solar altitude angle.

When looking at the radiant field experienced by pedestrians, described by the Mean Radiant Temperature (MRT), deep canyons are usually a desirable option. Several works have shown that the outdoor comfort conditions perceived by pedestrians are better in canyons oriented along the N-S direction and with H/W > 2 [5-8]. Other authors suggest H/W > 1.5 to reduce summer heat stress

for pedestrians [9]. Typically, in urban simulations, one assumes that urban canyons have a uniform (average) H/W ratio. However, real cities often present irregular building patterns: recent studies have shown that urban canyons with variable aspect ratios and diversity in urban form may reduce air temperature by 1.0 °C to 4.0 °C if compared to uniform urban canyons, while also providing benefits in terms of pedestrian thermal comfort [10-11].

Another relevant issue in the definition of the thermal field inside urban canyons is the role played by the albedo of the outer finishing layer of the buildings. Light colours, or any kind of coating with a high albedo, avoid the overheating of the outer surfaces, thus reducing the energy needs for space cooling and improving indoor thermal comfort in the summer. Moreover, low outside surface temperatures reduce the heat released by convection and by long-wave radiation from the buildings to the urban canyon. The application of high-albedo finishing layers to a single building can induce local effects on pedestrians [12], while positive effects at city scale can be observed only if this solution is applied at an urban scale. However, recent studies have shown an unexpected drawback: the short-wave radiation that is not absorbed by the facades is reflected towards the ground, thus hitting the pedestrians and overheating the ground surface [13]. In many cases, this side effect counterbalances the positive effects commented above and worsens the outdoor thermal comfort conditions [14-17]. Canyons with high aspect ratio emphasize the negative effect stemming from multiple reflections when the facades have a high albedo: some authors found out that an average albedo for the facades ($r \approx 0.4$) is the best compromise [18]. Other authors highlighted the same negative effect for cool pavements: although their higher albedo reduces near-surface air temperatures, they worsen thermal comfort for pedestrians, especially in open spaces [19-20].

Now, when it comes to dynamic energy simulations of buildings in an urban context, it is also important to determine the variation of the air temperature locally induced by the built environment, which is identified as the *Urban Heat Island* (UHI) effect. As amply witnessed in the literature, air temperatures in urban areas tend to be higher than those measured simultaneously in a nearby rural context, especially in the afternoon and at night [21-25]. Neglecting the urban heat island effect can lead to a remarkable underestimation of the cooling load of buildings, but also to an overestimation of their heating load [22, 26-29]. Unfortunately, available weather data are often referred to rural sites (e.g. airports), and as such, they are not suitable to be directly used in the simulation of buildings located in urban areas. With the purpose of adapting existing weather datasets to urban conditions, a range of approaches has been developed.

Outdoor comfort simulation tools and their capabilities have been assessed in previous research [30], revealing that the most commonly used tools in the research domain are ENVI-met, SOLWEIG (Solar and Long-Wave Environmental Irradiance Geometry), the RayMan model, and

the UTCI calculator. These tools have been applied to compute climatic conditions that range from urban canyons to city scale. However, ENVI-met is by far the one most frequently used by researchers to investigate the intertwined relation between the built environment, outdoor thermal comfort and air temperature in urban areas [31-34]. ENVI-met is a holistic three-dimensional non-hydrostatic tool for simulating the interactions among surfaces, air and plants, at high spatial (from 0.5 m to 5 m) and temporal (from 1 s to 5 s) resolution, that needs some user-defined boundary conditions (dry-bulb air temperature, relative humidity and wind velocity namely).

Despite its extensive use, ENVI-met has some drawbacks that can limit its usefulness in some applications. In particular, it does not manage complex geometries, namely those not meeting at right angles and does not account for heat storage of walls, which may result in underestimating air temperature values at night. Further, simulation times can easily exceed 24 h when the required spatial and time resolutions are high. To overcome these drawbacks, some scholars first generate suitable weather files with ENVI-met, and then use them to run simulations with other tools such as EnergyPlus for selected days only [35].

However, in the last five years, the Ladybug Tools suite came into the scene. It was initially developed and used for running extensive parametric analysis of different design choices at a restricted scale such as a single room or a building [36-37].

The possibility of modelling outdoor comfort was examined later, with the addition of a set of tools embedded in the Grasshopper environment. These provide reliable results within a reasonable computational time when the aim is the definition of average urban canopy conditions in terms of air temperature and relative humidity values [38-39], or the optimization of outdoor comfort conditions for different geometric layouts [40].

The potential of different climate control strategies for an idealized urban canyon has been assessed as well by coupling various software capabilities in Grasshopper [41], but without simultaneously accounting for the outdoor and indoor thermal fields. This is a step forward since outdoor comfort tools and building energy modelling tools are generally unconnected.

Practitioners can now appreciate the thermal influence of the outdoor space towards the interior, and vice-versa.

The Grasshopper tools are also freely available and more accessible to building designers working in the Rhinoceros CAD environment: this is a relevant issue for a wider diffusion of environmentally conscious design practices for urban areas. Given its novelty, the workflow still needs extensive validation. Some preliminary research found that the workflow offers good agreement with measured data [42], but further tests are needed.

In this framework, the present paper describes a novel simulation workflow that aims at conjugating all previously discussed aspects. The workflow is implemented in the Grasshopper platform and relies on several plug-ins to allow the simulation of indoor and outdoor thermal field. In particular, Dragonfly runs the Urban Weather Generator (UWG) tool, which estimates the hourly air temperature and relative humidity in the urban canopy starting from a rural weather file and generates a morphed weather file in the ".epw" format, compatible with many Building Energy Simulation tools [43-44].

On the other hand, Honeybee and Ladybug take into account the interaction of the envelope with both the indoor and outdoor spaces: they calculate the energy demand for space heating and cooling based on the EnergyPlus engine, while also assessing the outdoor mean radiant temperature in the canyon. Eventually, the workflow measures the thermal comfort perceived by pedestrians through suitable metrics, i.e the Mean Radiant Temperature (MRT) and the Universal Thermal Climate Index (UTCI), defined in Section 2.

The proposed workflow is tested on a real urban canyon in the city of Catania, Southern Italy. The reliability of the workflow in predicting the outdoor mean radiant temperature in the canyon is verified by comparison with experimental values taken in two different days under sunny and shaded conditions, respectively. The workflow is then used to estimate the energy demand of the buildings along the canyon, and to assess the effects of different albedo values for the envelope in terms of building thermal load and outdoor comfort.

The paper is organized as follows. Section 2 presents the workflow and describes the main algorithms used to account for the Urban Heat Island effect, to calculate the outdoor Mean Radiant Temperature and to measure the outdoor thermal comfort. Section 3 shows the case study and discusses the settings needed to implement it in the workflow; moreover, the experimental campaign is presented. Then, Section 4 discusses the results of the experimental campaign and the comparison with the simulated values. Section 5 presents the results of a parametric analysis aimed to emphasize the role of the albedo. Finally, Section 6 discusses the main limitations of the proposed workflow and suggests future lines of research.

2. Methodology

This Section addresses a series of methodological issues, concerning the algorithms used by the Grasshopper tools to assess the outdoor thermal comfort (see Section 2.1 and 2.2) and to estimate the hourly air temperature in the urban canopy (see Section 2.3). Finally, Section 2.4 discusses the structure of the workflow developed in this work in the Grasshopper environment, which allows simulating simultaneously the intertwined effects occurring in urban canyons.

2.1 Calculation of the Mean Radiant Temperature

Dealing with the prediction of the Mean Radiant Temperature (MRT) in an urban canyon is a complex task, due to the superposition of a long-wave and a short-wave radiant field [30]. The first one originates from the thermal emission of the built surfaces towards the human body; the second one is due to the solar radiation hitting the human body, both directly and after being reflected by the surfaces of the canyon.

To account for both radiant fields, the Ladybug Tools make use of an algorithm called *SolarCal*, recently developed at UC Berkeley [45]. According to this algorithm, a first calculation of the MRT is based on the only long-wave component, as in Eq. (1):

$$MRT_{LW} = \left(\sum_{i=1}^{N} F_i \cdot T_i^4 \right)^{1/4} - 273.15 \quad (°C) \tag{1}$$

Here, F_i are the view factors between the human body and the surrounding surfaces, calculated for each point of a user-defined grid, located at a certain height in the street canyon, and T_i is the temperature of these surfaces. The surface temperatures are calculated preliminarily through an EnergyPlus run, while the view factors are assessed through a *ray-tracing* approach [30], i.e. by tracing the path of light from the human body to the 3D scene and back to the light sources (the sun and the sky namely). Then, the contribution of the short-wave radiation and of the radiation coming from the sky vault adds to the MRT_{LW} as in Eq. (2) and Eq. (3).

$$T_{sky} = \sqrt[4]{\frac{L_{sky}}{0.95 \cdot \sigma}} - 273.15 \quad (°C) \tag{2}$$

$$MRT = MRT_{LW} \cdot \left(1 - \frac{F_{sky}}{2} \right) + T_{sky} \cdot \left(\frac{F_{sky}}{2} \right) + \frac{ERF}{h_r \cdot f_{eff}} \quad (°C) \tag{3}$$

In Eq. (2), L_{sky} is the horizontal infrared radiation intensity, whose value is available in the Typical Meteorological Year (TMY) weather file, and $\sigma = 5.67 \cdot 10^{-8}$ $W \cdot m^{-2} \cdot K^{-4}$ is the Stefan-Boltzmann

constant. In Eq. (3), the radiant heat transfer coefficient is constant and set to $h_r = 6.012\ W \cdot m^{-2} \cdot K^{-1}$. The fraction of the body surface exposed to diffuse radiation from the environment is constant and set to $f_{eff} = 0.696$ by default (seated person). Actually, for a standing person this value should be 0.725 [46], but the only way to modify it consists in writing it manually directly into the Python code. Since this value affects the short-wave irradiance received by the human body and, consequently, the MRT, in this work $f_{eff} = 0.725$ has been set for pedestrians by modifying the Python code.

In Eq. (3), ERF is the so-called *Effective Radiant Field*, i.e. the overall short-wave irradiance absorbed by the human body. More details about the calculation of the ERF are available in the literature [45, 47], but it is important to highlight the main simplifying assumptions behind its calculation:

- the fraction of the human body exposed to direct beam solar radiation varies with solar altitude and azimuth, and is taken from the ASHRAE Standard 55 [48];
- the short-wave absorptance of the human body is set by default at 0.7, but it can be modified by the user;
- the total solar irradiance hitting the ground is reflected proportionally to the ground albedo, and this reflected radiation hits only the lower half of the human body;
- the solar irradiance reflected by the façades of the buildings, and then hitting the human body, is not taken into account.

2.2 Calculation of the Universal Thermal Climate Index

The Universal Thermal Climate Index (UTCI) is a widely accepted parameter used to measure the thermal stress experienced by people when outdoors. Its calculation rests on the model developed by Fiala to describe the complex physiological behaviour of a human body, including its thermoregulatory reactions to modifications in the outdoor conditions. In particular, the UTCI is the value of the air temperature that, under suitably defined reference conditions, causes in the human body the same physiological response as in the actual conditions [49]. The reference conditions consider a person walking at 4 km/h, with a metabolic rate corresponding to 2.3 met. Moreover, the reference wind speed is 0.3 m/s at 1.1 m, and the reference relativity humidity is 50%. Finally, the reference mean radiant temperature equals the dry-bulb air temperature. The value of the UTCI depends only on the air velocity, the mean radiant temperature, the relative humidity and the actual air temperature. The calculation is performed through an extensive polynomial expression with 210 coefficients [49]. The UTCI can also be calculated through the following simplified equation [50]:

$$UTCI = 3.21 + (0.872 \cdot T_a) + (0.2459 \cdot MRT) - (2.5078 \cdot v_a) - (0.0176 \cdot RH) \quad (°C) \qquad (4)$$

According to the UTCI value, it is possible to classify the thermal stress experienced by a pedestrian as detailed in Table 1.

Table 1 – Correlation between thermal stress and UTCI

UTCI range	Stress category
UTCI > 46 °C	Extreme heat stress
46 °C ≥ UTCI > 38 °C	Very strong heat stress
38 °C ≥ UTCI > 32 °C	Strong heat stress
32 °C ≥ UTCI > 26 °C	Moderate heat stress
26 °C ≥ UTCI > 9 °C	No thermal stress
9 °C ≥ UTCI > 0 °C	Slight cold stress
0 °C ≥ UTCI > -13 °C	Moderate cold stress
-13 °C ≥ UTCI > -27 °C	Strong cold stress
-27 °C ≥ UTCI > -40 °C	Very strong cold stress
UTCI ≤ -40 °C	Extreme cold stress

2.3 Weather data morphing

The UHI effect is influenced not only by the shape and aggregation pattern of the buildings but also by anthropogenic activities such as traffic, street lighting and building operation, which define the amount of heat released to urban canyons.

A convenient approach to account for such phenomenon is that of creating suitable weather datasets through modification (i.e. morphing) of existing weather data collected at rural sites and made available in the ".epw" format, which is compatible with many building simulation tools. The Urban Weather Generator (UWG) builds upon these premises and is able to estimate the hourly urban canopy air temperature and relative humidity considering the heat exchange and the air stratification at different atmospheric layers [43-44].

However, the morphing procedure does not modify weather variables such as the global horizontal solar irradiance and the wind velocity, which are then retained from the original rural TMY weather file. While the first hypothesis is acceptable, since the solar irradiance available on a horizontal unobstructed surface does not change significantly from a rural to an urban site nearby, the second one clearly brings some inaccuracies because the wind pattern is definitely modified in urban environments.

Apart from the meteorological variables gathered from a traditional rural TMY file, UWG requires information about the urban morphology to calculate the average building height, the site coverage ratio (i.e. the ratio of the buildings footprints to the urban site area) and the façade-to-site ratio (i.e.

the ratio of the buildings facades to the urban site area). These parameters are derived from the 3D model of the district, built on Rhinoceros.

For what concerns the sensible heat fluxes released by heat sources within the urban area, the UWG splits the component due to vehicles, street lighting and pedestrian activity from that due to buildings, i.e. the heat released from HVAC systems: the user has to define both contributions separately. Finally, the optical and thermal parameters of all the built surfaces (streets, pavements, facades and roofs) are required to estimate the absorbed short-wave solar radiation and the emitted long-wave radiation within the Urban Boundary Layer (UBL). These values are meant as an average at an urban scale and can be easily assigned through the graphical interface provided by the Dragonfly tool within Grasshopper environment, thus perfectly fitting with the other components of the proposed workflow.

Several works concerning the use of the UWG tool for predicting the UHI effect in real cities have shown that the urban morphology is the issue with the greatest influence on the outcomes [26, 51]. The comparison with experimental measurements confirmed the ability of the tool to capture the average trend of the urban air temperature in different climates, thus improving the accuracy of building energy simulations in urban contexts [43-44, 51].

2.4 Presentation of the simulation workflow in Grasshopper

A schematic of the workflow developed and tested in this research is shown in Figure 1, where the connections amongst the different tools are highlighted.

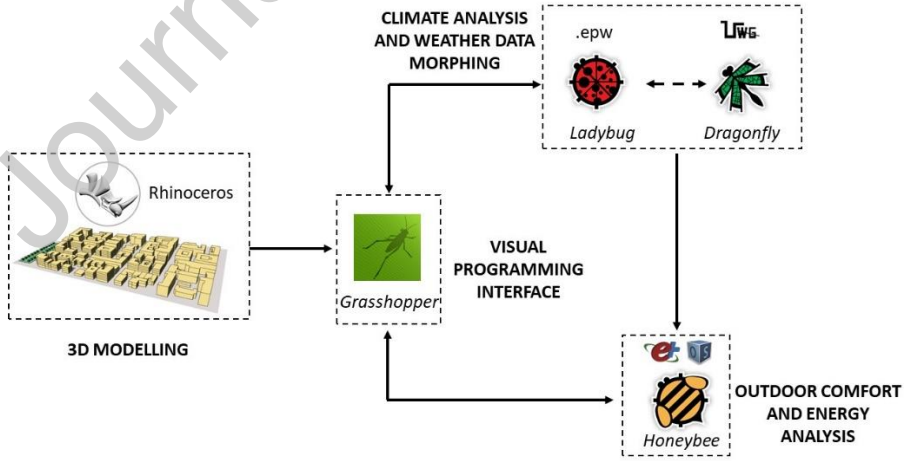

Figure 1 – Schematic of the simulation workflow in Grasshopper.

The first step of the proposed simulation workflow consists in creating an appropriate geometric representation of the urban area being investigated. In this sense, Gimenez et al. suggest that buildings are represented as block models from footprints extrusion [52]: this level of detail,

corresponding to "level one" according to the CityGML standardised data model format, is accurate enough for thermal modelling purposes. However, the presence of protrusions and recesses such as balconies and porches can affect both outdoor microclimate and buildings energy needs because of their shading effect. Consequently, in this study, the buildings facing the canyon are modelled with a level of detail "two", including all these architectural elements as well with the exclusion of pitched roof structures that have been modelled as flat, whereas all the surrounding buildings – whose features influence the morphing procedure with the UWG – are modelled by just extruding their footprints.

Then, thermal zones can be defined for the selected buildings, starting from the 3D model generated so far, through the *Mass2Zone* component. After defining the geometric features of the thermal zones, the energy demand of the buildings facing the canyon is calculated by running EnergyPlus simulations via the OpenStudio interface. To this aim, the following Honeybee components are exploited: i) *setEPZoneLoads* for assigning design values for internal loads, due to occupants, lighting and equipment; ii) *setEPZoneSchedules* for defining suitable time schedules for infiltration rates, setpoint temperatures and internal loads; iii) *HVACSystem* for linking zone information with HVAC specifications. Finally, the resulting *_HBZones* are linked to the *exportToOpenstudio* component: the latter is also connected with the *_epwWeatherFile* resulting from the morphing procedure with Dragonfly and the *_analysisPeriod* component that sets the simulation run period.

It is worth noting that such an approach does not simulate any specific mechanical system but rather returns the building energy demand for heating and cooling respectively.

The outputs of the simulations include all the outside surface temperatures for the thermal zones, which are needed in the calculation of the outdoor MRT. To this aim, one also needs to model a "ground thermal zone", i.e. a fictitious volume without any internal gains and delimited by soil on each side except for its roof, the latter corresponding to the street surface. This step allows calculating the surface temperature of every single area of the ground inside the urban canyon, as a function of the shadows cast by other objects and of the heat storage in the ground surface. Through the *genTestPts* component (see Phase 1 in Figure 2), the street surface is divided into a grid, setting the pitch to 1 m to get an accurate spatial resolution (*_gridSize*). Then, all the created surfaces delimiting the ground zone are jointed with *Join* and *CapEx* components and, eventually, the ground zone is formed through *Mass2Zone* and *CreateEPGround* (see Phase 2 in Figure 2). In this stage, it is also possible to set the thermal and optical properties of the paving material through the *EPOpaqueMat* component; in our case, the solar absorptance is set to 0.8, meaning that the albedo is $r = 0.2$, which is a reliable value for weathered asphalt [14, 16].

The further step consists in defining a grid of points parallel to the canyon surface, placed at 1.1 m above the ground. For each point of this grid, the *IndoorViewFactor* component calculates the view factors with every surface of the canyon through a ray-tracing approach. The output of this component (*viewFactorMesh* and *viewFactorInfo*, see Phase 3 in Figure 3) is used by the *OutdoorComfRecipe* component, which also receives information about the outdoor surface temperatures previously calculated by OpenStudio (*readEPSrfResult*) in order to generate an output called *comfRecipe*. The latter is a matrix containing all the essential variables for defining MRT and UTCI metrics, such as air temperature, wind speed, relative humidity, view factors, scattered solar radiation, direct solar radiation and horizontal global radiation. The wearing absorptance (*cloAbsorptivity*) is set to a default value (0.7) if no input is given.

Finally, the *MicroclimateMap* processes the data contained in the *comfRecipe* and generates the MRT and UTCI maps for the user-defined period (*analysisPeriodOrHOY* input, see Phase 4 in Figure 3) through the *mtx2DataTree* component.

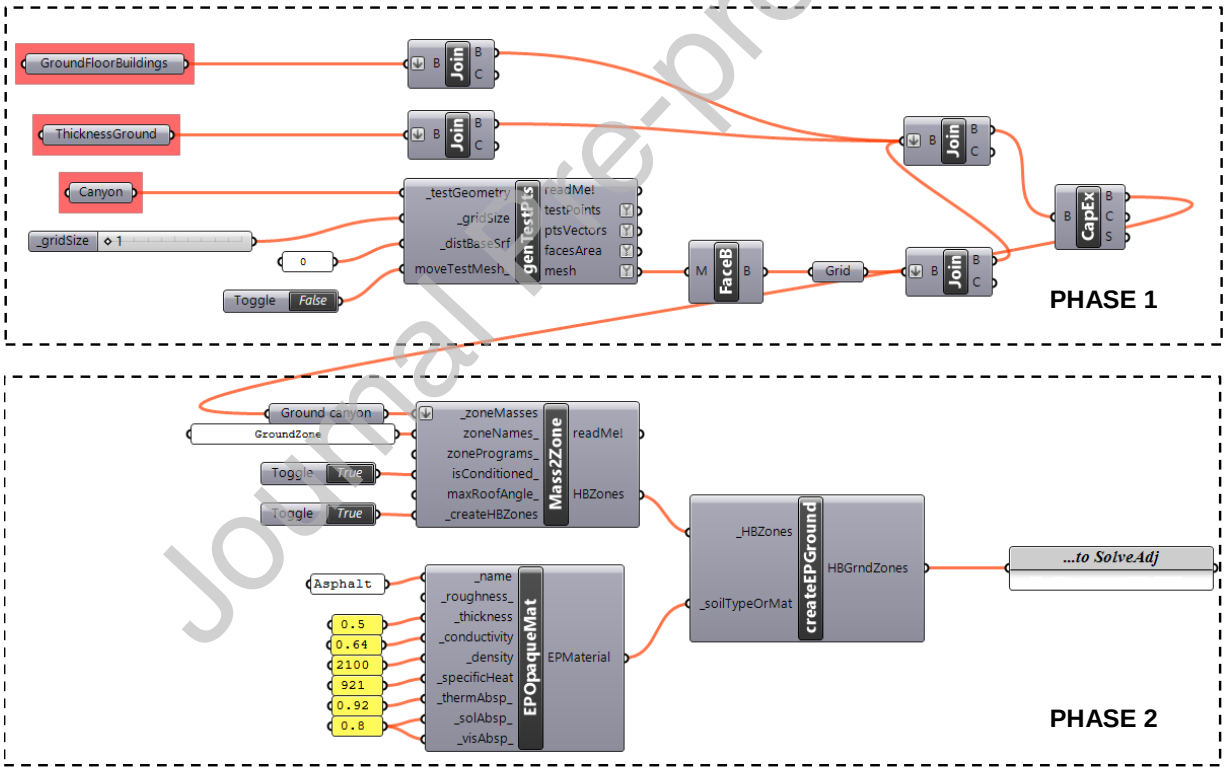

Figure 2 – Grasshopper components to create a Ground zone

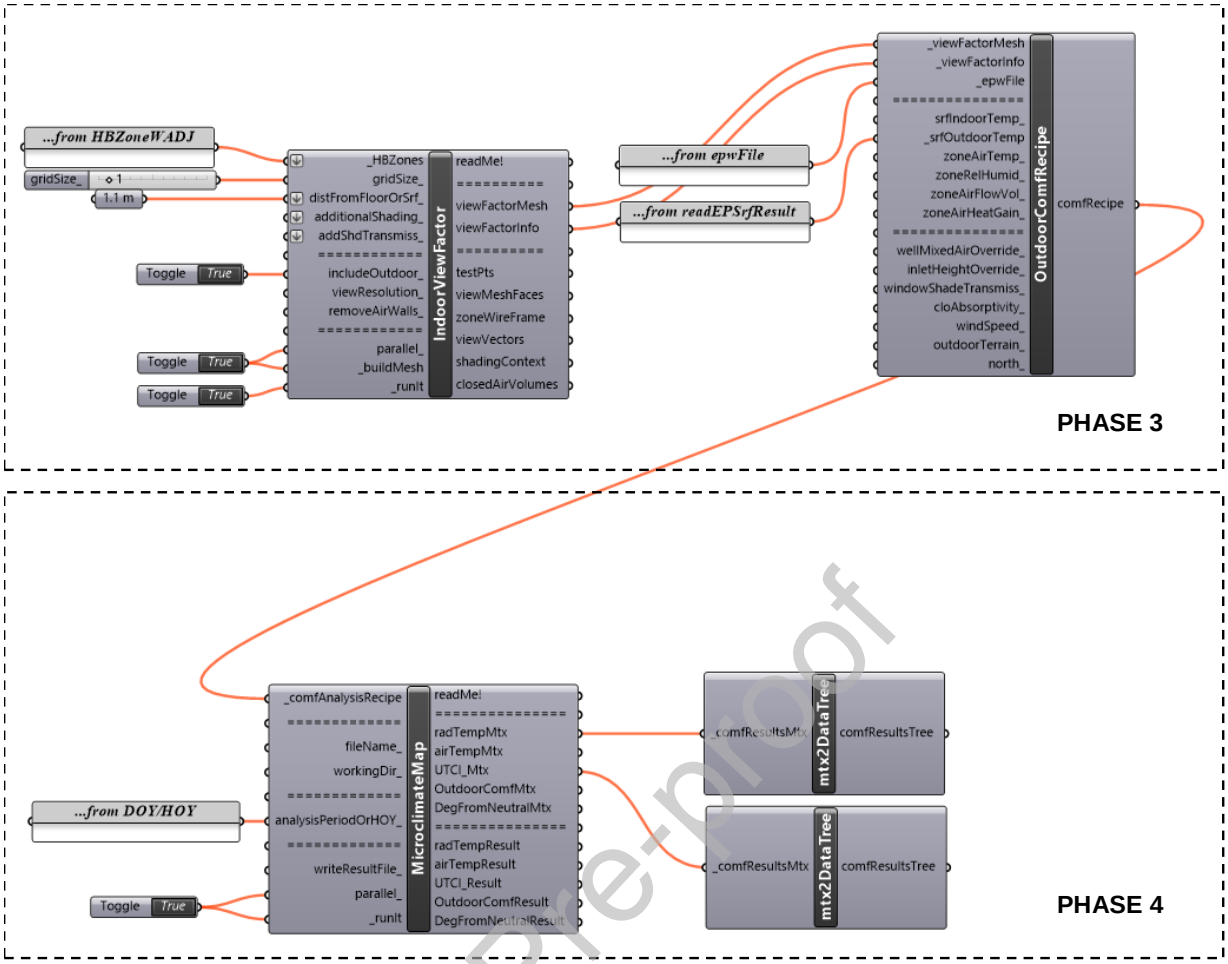

Figure 3 – Grasshopper components to obtain MRT and UTCI maps

3. Case study and experimental measurements

3.1 The selected urban canyon

The urban canyon selected to test the proposed workflow is located in the centre of Catania, a densely populated city in Sicily. Figure 4 shows the entire area addressed by this study, which belongs to a district next to the historic centre. The selected area has a side of about 375 m, and includes multi-storey residential buildings (from two to seven floors) built between the 1930s and the 1960s, which represent the most diffuse residential typology in the city. All the buildings in the selected area are modelled as blocks by extruding the footprints in Rhinoceros: this makes Dragonfly able to calculate the geometric parameters needed by UWG for the morphing of the weather file.

Within this area, a specific urban canyon is then identified as shown in Fig. 4, namely the portion of Via Ughetti included between Via Tommaso Grossi and Via Macallè. This street has been chosen because it is usually crossed by many people and cars during weekdays, thus it can be considered representative of the crowded city center.

The length of the canyon is of around 80 m, with a mean building height of 11 m. The canyon has an aspect ratio H/W = 1.14 and is oriented along the East-West direction. Due to the relatively low aspect ratio and the unfavourable orientation, the canyon is expected to show high mean radiant temperatures and marked outdoor thermal discomfort in the summer. The buildings facing this street are modelled as thermal zones in EnergyPlus (one zone per floor), in order to calculate their energy needs for heating and cooling. Balconies and window surfaces, inclusive of the surrounding frames, have been added to these buildings. The surrounding buildings, shown in a light grey colour in Fig. 4, act as shading surfaces.

From the thermal point of view, some simplifications are introduced. As concerns the outside walls, all the buildings are assumed to have 60-cm thick walls made with basalt stones laid with lime mortar, and finished with two 30-mm layers of plaster, with an average U = 1.18 $W \cdot m^{-2} \cdot K^{-1}$. This type of walls, with a very high surface mass (around 1200 $kg \cdot m^{-2}$), is widespread for pre-1960s buildings in Catania. The windows are single-glazed and with wooden frames (U_w = 4.8 $W \cdot m^{-2} \cdot K^{-1}$), apart from few openings recently refurbished. Slabs are instead made up of reinforced concrete and hollow bricks, and finished externally by tiles and internally by cement plaster, with a resulting U-value of 1.30 $W \cdot m^{-2} \cdot K^{-1}$.

On the other hand, the parameters needed for running the morphing procedure in UWG are listed in Table 2. All the buildings are considered as "mid-rise apartments built before the 1980s" according to the DOE benchmark buildings categorization [53]. The fraction of heat released by the air conditioning units to the canyon has been set to 0.5, meaning that the remaining 50% of the heat waste is released above the roofs, and thus it does not affect the canopy layer. The anthropogenic heat due to traffic has a peak value of 10 W/m^2 and average daily values of 5.5 W/m^2 during weekdays and 4 W/m^2 during weekends [44]. As for the albedo of walls and roofs, the values reported in Table 2 refer to typical colours and finishing materials used in Catania; the vegetation albedo is a standard value taken from Ref. [43]. The remaining parameters are either automatically calculated by the software (e.g. geometrical features retrieved from the geometric model) or set according to the suggested default values [43]. The tree and grass coverage ratio are estimated starting from observation on-site.

Figure 4 – Selected urban area (left-hand picture) and its geometrical model in Rhino (right-hand picture)

Table 2 – Input parameters for the morphing procedure with UWG

User's input	Building typology: mid-rise apartments (pre-1980s)	
	Heat fraction released to the canyon	0.5
	Road albedo	0.2
	Vegetation albedo	0.25
	Walls albedo	0.4
	Roofs albedo	0.3
	Sensible anthropogenic heat (peak value)	10 W/m^2
	Glazing ratio	0.15
Calculated by Dragonfly	Average building height	11 m
	Site coverage ratio	0.39
	Facade-to-site ratio	1.19
	Tree coverage ratio	0.01
	Grass coverage ratio	0.04
Default values	Daytime height for the Urban Boundary Layer	1000 m
	Nighttime height for the Urban Boundary Layer	50 m
	Inversion height	150 m
	Circulation coefficient	1.2
	Exchange coefficient	1

3.2 Measurement of the environmental parameters

A TESTO 480 data logger was placed in Via Ughetti sufficiently close to the centre of the street, as in Figure 5; the data logger was equipped with suitable probes to measure the parameters needed in the experimental campaign, as reported in Table 3.

The hot-wire anemometer was placed at the height of 1.5 m from the ground, and measured the velocity component along the axis of the canyon. The ground temperature was measured through a type-K thermocouple pressed against the asphalt. All the other probes, including the black globe thermometer, were positioned at the height of 1.1 m from the ground. All values were recorded

every 30 s; however, suitable average values over longer periods were calculated during post-processing when necessary.

Table 3 – Parameters measured by the probes and corresponding accuracy

Measured parameter	Probe	Measurement range	Accuracy
Dry-bub temperature	TESTO 0632 1543	0 – 50 °C	± 0.5 °C
Relative humidity	TESTO 0632 1543	0 – 100 %	± 2 %
CO_2 concentration	TESTO 0632 1543	0 – 10000 ppm	± 50 ppm
Black globe temperature	TESTO 0602 0743	0 – 120 °C	± 1.5 °C
Wind speed	TESTO 0635 1543	0 – 20 m/s	± 0.03 m/s
Ground temperature	K-type thermocouple	0 – 1100 °C	± 2 °C

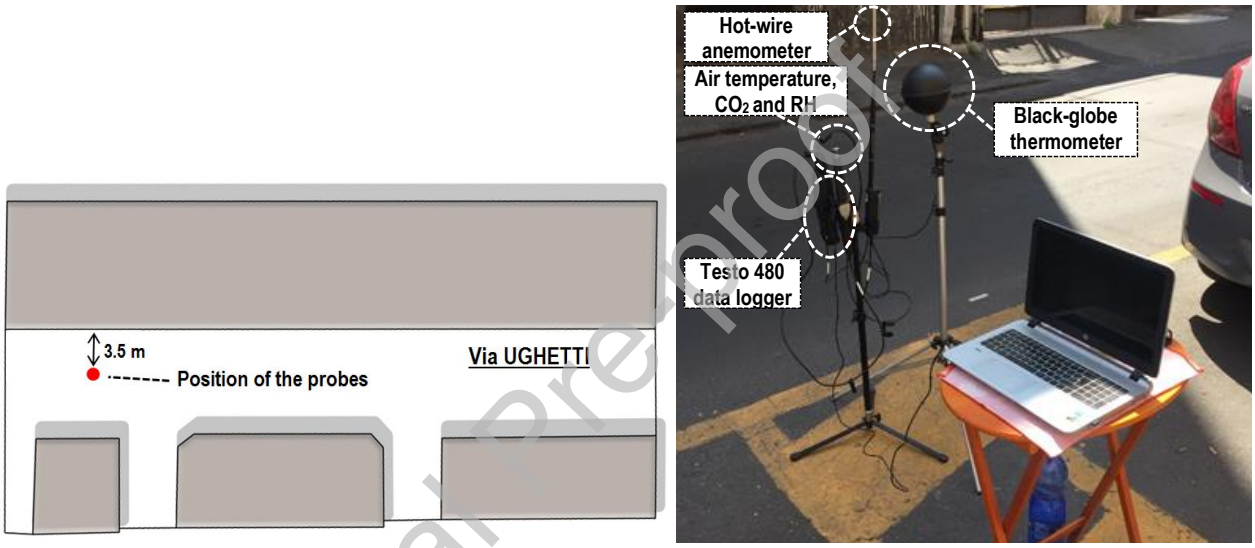

Figure 5 – Position of the probes in selected the urban canyon
(the picture on the right refers to the monitoring campaign on 30th August 2018)

A first monitoring campaign was performed on 30th August 2018 from 12:50 to 15:00; the measurement campaign was then repeated on 17th July 2019 from 11:00 to 17:00. In the first measurement campaign, the probes were in the shade for the most significant part of the time, while in the second campaign the probes were continuously kept under the sunshine, by also taking suitable actions to avoid an improper overheating of the probe while measuring the dry-bulb air temperature. The relatively short duration of the campaign is justified by the need to perform a first preliminary check and calibration of the simulation model. Based on the outcomes and the lessons learned from this experimental activity, longer and more detailed measurements will be performed for future investigations.

The campaign did not include the measurement of the solar irradiance, based on the assumption that – for any given hour of the day – the global horizontal solar irradiance mainly depends on the latitude of the site, and that its values can be retrieved from the TMY file. In order to check the

reliability of the values of global horizontal solar irradiance included in the TMY file for Catania Fontanarossa, Figure 6 compares them to those measured by the local agro-meteorological service [54] in the same two days of the measurement campaign. The plots suggest that the weather file underestimates the actual values, but the maximum discrepancy is less than 9% in early morning when the solar irradiance is low. On the other hand, in the central hours of the days, the discrepancy keeps between 3% and 6%. This comparison proves that the solar irradiance values included in the TMY weather files can be effectively used in the simulations.

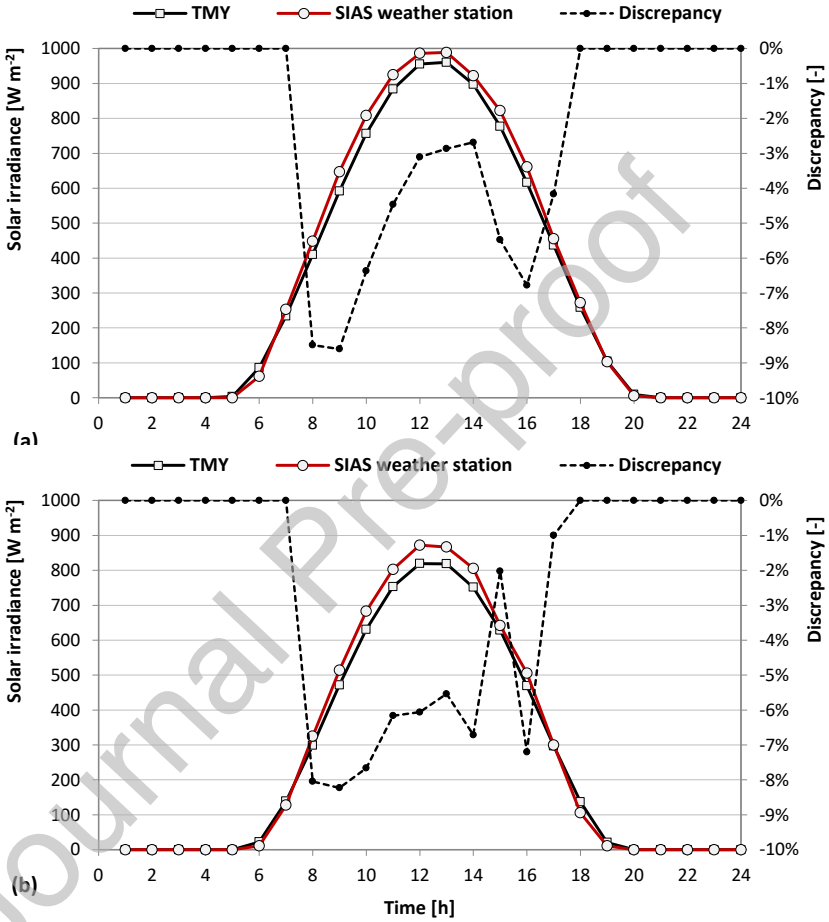

Figure 6 – Global horizontal solar irradiance: comparison between measured values and those contained in the TMY file for the same city (a: 17th July 2019, b: 30th August 2018)

3.3 Mean Radiant Temperature: experimental assessment

The Mean Radiant Temperature (MRT) allows the evaluation of the radiant heat exchange between the human body and the surroundings. In particular, the MRT is defined as "*the uniform temperature of an imaginary enclosure in which the radiant heat transfer from the human body equals the radiant heat transfer in the actual non-uniform enclosure"* [55].

The MRT can be measured on-site according to two main approaches. The first approach implies using a black (or grey) globe thermometer; the second one relies on an experimental apparatus

consisting of three pairs of pyranometers and three pairs of pyrgeometers, arranged along the three principal directions [56-58]. For its simplicity and portability, a black globe thermometer is used in this study. This is a hollow metal sphere painted in black, with a diameter of 150 mm; when the black globe thermometer is placed in the environment under investigation, the MRT can be correlated to the measured values of the globe temperature T_g and the air temperature T_a as follows [56]:

$$\mathrm{MRT} = \sqrt[4]{\left(\mathrm{T_g}+273.15\right)^4 + \frac{\mathrm{h_c}}{\varepsilon \cdot \sigma}\cdot\left(\mathrm{T_g}-\mathrm{T_a}\right)} - 273.15 \quad (°\mathrm{C}) \tag{5}$$

In Eq. (5), $\varepsilon = 0.95$ is the emissivity of the black globe. The convective heat transfer coefficient for the globe surface depends on the wind speed v_a as in Eq. (6), where $d_g = 0.15$ m is the globe diameter:

$$\mathrm{h_c} = 6.3 \cdot \frac{\mathrm{v_a^{0.6}}}{\mathrm{d_g^{0.4}}} \tag{6}$$

This measurement technique was initially conceived for indoor applications, but recent studies have shown that, despite a certain degree of approximation, the black globe thermometer is sufficiently reliable in outdoor applications if the calculation of the MRT is based on data averaged over at least ten minutes [58-59]. In fact, this allows to average out the effects of rapid changes in the wind speed and in the degree of cloud cover.

4. Results

This Section presents the outcomes of the experimental measurements and of the simulations performed in this study. In particular, Section 4.1 discussed the measurement campaign conducted in the urban canyon in two different days in summer, while Section 4.2 shows the results of the simulations and their comparison with the experimental MRT values. Finally, once the reliability of the simulation workflow has been verified, Section 4.3 discusses further simulated results concerning the time trend and the spatial variation of MRT and UTCI within the canyon.

4.1 Measured microclimatic parameters and Mean Radiant Temperature

This paragraph discusses the main results of the measurement campaigns carried out on 30th August 2018 and 17th July 2019 in the selected urban canyon. In particular, from Figure 7 it is possible to observe that on 30th August 2018 the relative humidity (RH) swings between 40% and 55%, which is very close to the reference relativity humidity assumed for the UTCI calculation (50%). The CO_2 concentration, even if affected by sudden variations, shows a decreasing trend from 380 ppm at

13:15 to 360 ppm at 15:00, due to the reduced number of vehicles travelling during this period of the day. No correlation between the single peaks in the CO_2 concentration and the cars passing by the street could be observed: indeed, the values recorded are lower than 400 ppm, which is a fairly typical value assumed as baseline for outdoor concentrations in cities, and do not refer to particulate matter, CO or other oxides coming from engine combustion processes.

Moreover, the wind speed along the canyon has a very irregular trend, which is a typical condition in urban canyons: in fact, the values can drop from 3.0 m/s to around 0.1 m/s in a few seconds.

The dry-bulb air temperature ranges from 29 °C to 31 °C during the first hour, but without a clear trend, while the ground temperature and the black globe temperature keep almost constant around 32°C. Starting from 14:10, a sudden increase is observed for all temperatures: this suggests that direct solar radiation now hits all the probes, while they were previously in the shade of a building. Now, this is acceptable for the black globe and the ground surface, since the solar radiation is expected to modify their temperature; on the contrary, the probe that measures the dry-bulb air should not be hit by the solar radiation. For this reason, in the second measurement campaign, the air temperature probe was duly shielded from the direct solar radiation. Accordingly, the calculation of the MRT for the first measurement campaign is limited to the period when both probes were shaded, that is to say, the only period when proper measurement conditions were ensured.

Figure 8 shows the time trend for all the parameters measured on 17th July 2019. Also, in this case, the dry-bulb air temperature oscillates quite randomly between 29 °C and 34 °C. RH shows lower values than in the first campaign, and ranges between 15% and 40%. As in the first campaign, the CO_2 concentration has sudden variations, but with a decreasing trend from 360 ppm at 11:00 to 330 ppm at 14:00 and then with a more stable trend around 345 ppm. The wind speed along the canyon fluctuates rapidly between 0.1 m/s and 3.0 m/s, with some peaks of about 4.0 m/s. The values averaged over ten minutes range between 0.6 m/s and 1.7 m/s.

Finally, the ground temperature keeps increasing from 36 °C at 11:00 to 42 °C at 13:45, as a result of the solar irradiance incident on the ground surface, which reaches its peak value around 13:00 (see Figure 6); afterwards, the ground temperature shows a constant decrease. The globe temperature has a less clear trend, since it is highly influenced by wind speed.

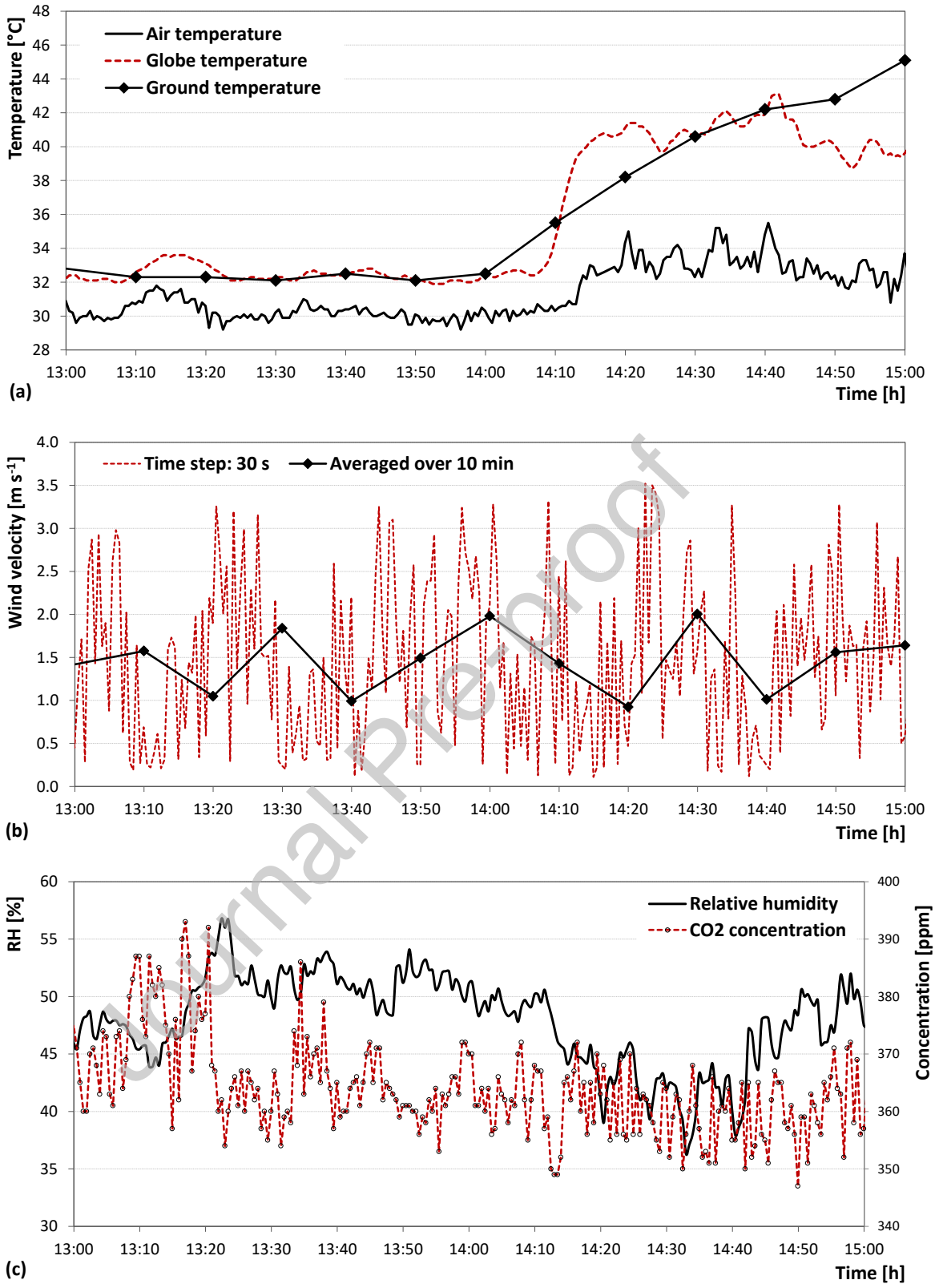

Figure 7 – Time trend of the parameters measured on 30th August 2018.
a: dry-bulb air temperature, black globe and ground temperature;
b: wind speed; c: relative humidity and CO2 concentration

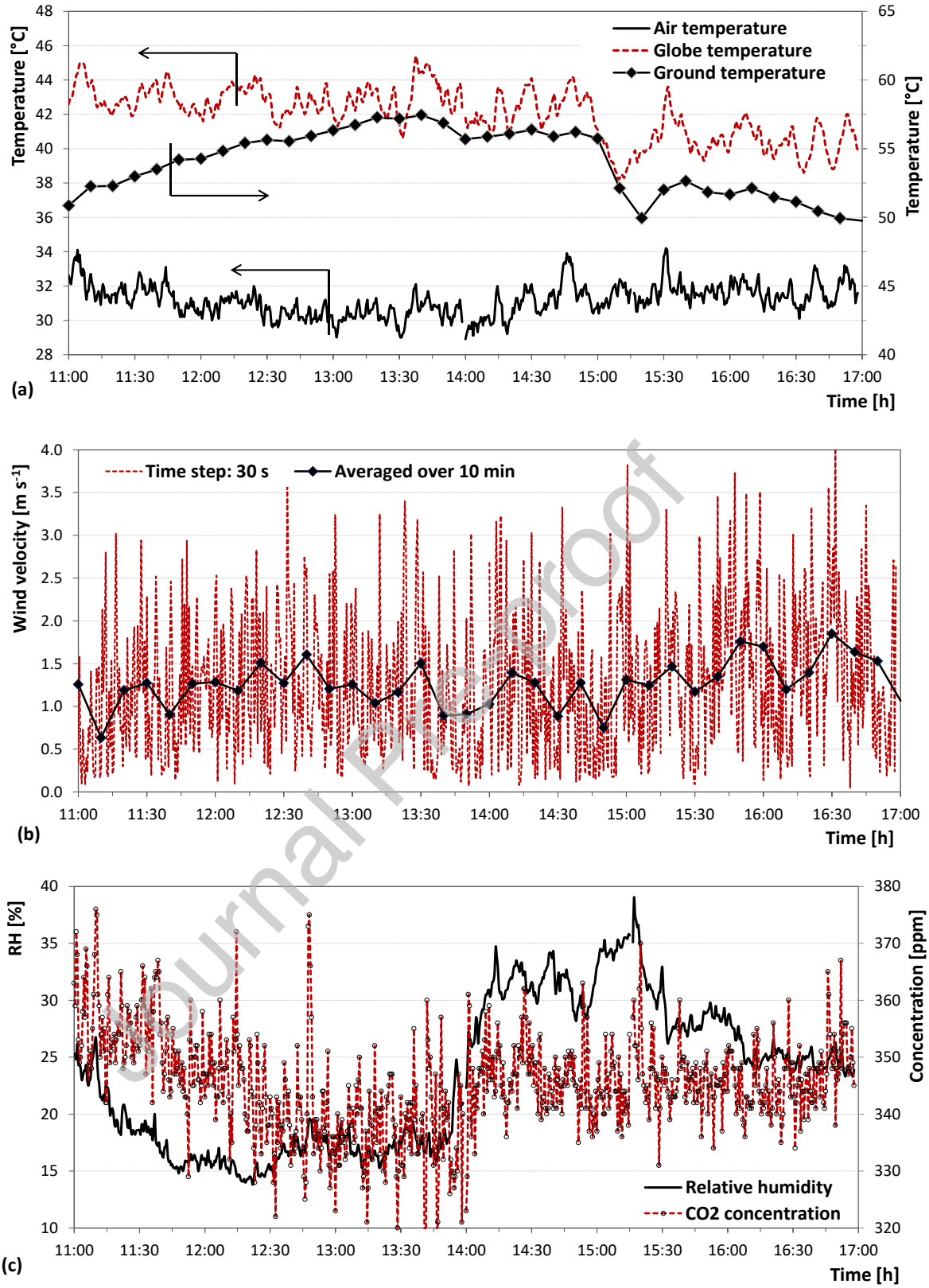

Figure 8 – Time trend of the parameters measured on 17th July 2019.
a: dry-bulb air temperature, black globe (left-hand axis) and ground temperature (right-hand axis)
b: wind speed; c: relative humidity and CO_2 concentration

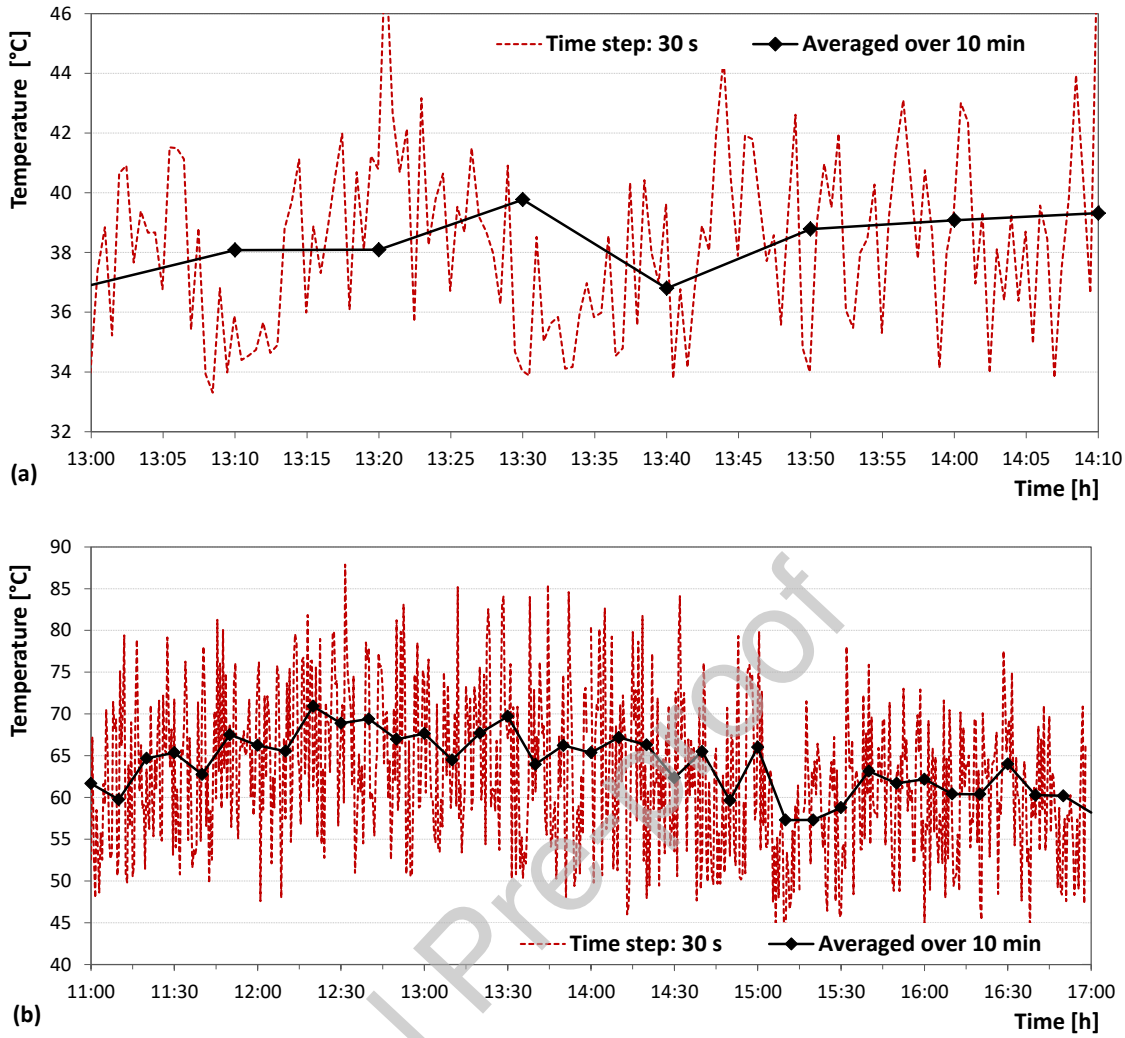

Figure 9 – Experimental Mean Radiant Temperature in the selected position. a: 30th August 2018; b: 17th July 2019

Now, based on the parameters measured by the probes, it is possible to calculate the experimental MRT through Eq. (5). This calculation can be performed at each time step, i.e. every 30 s; however, previous studies have shown that the black globe has non-negligible thermal inertia, which is not compatible with the sudden variations in the wind velocity outdoors [58-59]. Hence, it is appropriate to calculate the MRT on a higher time basis (10 minutes), by adopting in Eq. (5) the average of the values measured over this time-lapse.

The results for both calculation methods are reported in Figure 9, from which it is possible to understand the prominent role played by the direct solar radiation. Indeed, in the first measurement campaign, when the probes were in the shade, the MRT fluctuates between 36 °C and 40 °C; on the other hand, in the second measurement campaign, the direct solar irradiance determines a marked increase in the MRT, up to 70 °C at 13:30.

4.2 Calculation of the MRT and comparison with the experimental results

In order for the simulation model to calculate the MRT accurately in the same position where the probes have been located, it is essential to assign suitable albedo values to all the surfaces. Most of the buildings in the canyon show light colours, apart from building #6 (see Figure 10), which is painted in grey. This justifies the relatively high albedo chosen for the facades, reported in Table 4. Moreover, according to the literature, the albedo of asphalt varies between 0.05 and 0.2, depending on its colour: as previously highlighted, r = 0.2 is here adopted since this is a reliable value for weathered asphalt (Table 4).

Table 4 also includes the view factors calculated by the *IndoorViewFactor* component in relation to the long-wave radiant heat transfer from the surfaces of the canyon to the point of measurement, placed at 1.1 m above the ground. These values suggest that the main contribution to the long-wave MRT comes from the ground surface: in particular, a higher contribution to the MRT is expected from the zones close to the point of measurement. However, the buildings other than #1 and #4 play a negligible role in the MRT calculation. The sky view factor is also relevant since it amounts to 0.152.

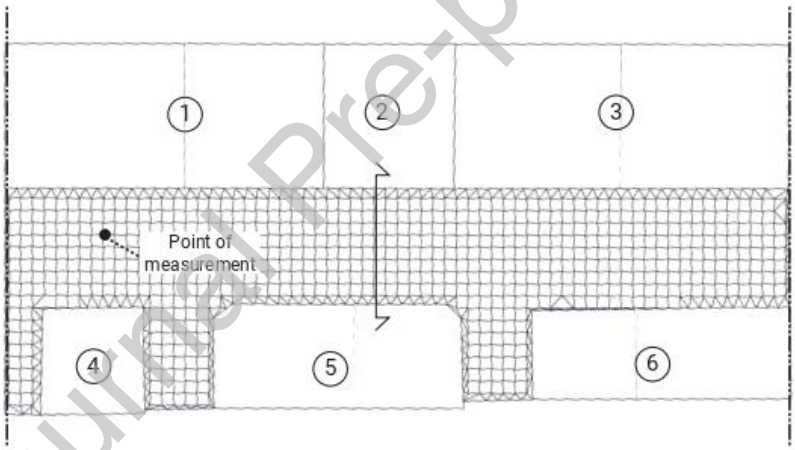

Figure 10 – Identification of the surfaces in the urban canyon (the central section is used to plot the MRT profile in Figure 11)

Table 4 – View factors from the point of measurement to the facades, and corresponding albedo

Facade	Colour	r	View Factor	Facade	Colour	r	View Factor
#1	White/yellow	0.70	0.243	**#5**	Light brown	0.50	0.015
#2	Light brown	0.55	0.002	**#6**	Grey	0.40	$\approx 10^{-4}$
#3	Light grey	0.60	$\approx 10^{-4}$	**Ground**	Dark grey	0.20	0.451
#4	Light grey	0.60	0.090	**Sky**	-	-	0.152

As a final point, in order to check the reliability of the Ladybug Tools in the calculation of the outdoor MRT, the ".epw" file read by the *OutdoorComfRecipe* (Figure 3) was modified – through

the *Elements* software tool [60] – by imposing the same time profile of outdoor temperature, relative humidity and wind speed measured in the urban canyon by the probes.

This would ensure that discrepancies between measurements and predictions should be attributable to the geometry of the canyon, the thermal properties of the materials and the inherent algorithms, but not to inappropriate weather data.

The main results of this first simulation step are reported in Table 5 and Table 6, which compare measured and simulated values for the ground surface and the MRT. The simulated ground surface temperature refers to the grid element corresponding to the position of the surface temperature probe on the ground.

Starting from Table 5, which refers to the first experimental campaign (probes in the shade), it is possible to observe that the results of the simulation show a promising agreement with the measured values. Indeed, the absolute value of the discrepancy for the MRT is 0.6 °C at 13:00 and only 0.3 °C at 14:00. The ground surface temperature resulting from the simulations slightly underestimates the measured value; however, this discrepancy is below the accuracy of the K-type thermocouple used to this aim.

When it comes to the results of the second experimental campaign, the absolute errors significantly increase because of the presence of direct solar radiation (Table 6). The simulated values of both the ground surface temperature and the MRT tend to be higher than the measured values, especially around solar noon, which in summer occurs at 13:00 due to the daylight savings time.

Table 5 – Measured and simulated values for ground surface temperatures and MRT (30th August 2018)

	Time	**13:00**	**14:00**
Ground surface	Measured	33.6 °C	36.2 °C
	Simulated	32.8 °C	35.5 °C
	Difference	- 0.8 °C	- 0.7 °C
Mean Radiant Temperature	Measured	36.9 °C	39.1 °C
	Simulated	36.3 °C	39.4 °C
	Difference	- 0.6 °C	+ 0.3 °C

Table 6 – Measured and simulated values for ground surface temperatures and MRT (17th July 2019)

	Time	**11:00**	**12:00**	**13:00**	**14:00**	**15:00**	**16:00**	**17:00**
Ground surface	Measured	50.9 °C	53.3 °C	55.6 °C	56.9 °C	56.0 °C	51.7 °C	50.8 °C
	Simulated	54.4 °C	57.5 °C	59.6 °C	60.5 °C	59.9 °C	54.8 °C	50.7 °C
	Difference	+ 3.5 °C	+ 4.2 °C	+ 4.0 °C	+ 3.6 °C	+ 3.9 °C	+ 3.1 °C	- 0.1 °C
Mean Radiant Temperature	Measured	61.7 °C	66.3 °C	67.7 °C	65.4 °C	66.0 °C	62.2 °C	58.2 °C
	Simulated	63.8 °C	67.8 °C	73.8 °C	71.4 °C	70.2 °C	64.5 °C	57.6 °C
	Difference	+ 2.1 °C	+ 1.5 °C	+ 6.1 °C	+ 6.0 °C	+ 4.2 °C	+ 2.3 °C	- 0.6 °C

By looking at the results of Table 6, one can reasonably infer that the proposed workflow shows a marked difficulty in determining the ground surface temperature under direct solar radiation, most probably due to an inappropriate simulation of the heat conduction and storage phenomena in the ground. Choosing a lower albedo for the asphalt would even increase the discrepancy between measured and simulated ground surface temperatures. These issues have an effect also in terms of MRT prediction: here, other possible sources of discrepancy are the simplified algorithms used to treat the direct solar radiation reflected by the building surfaces and by the ground.

The results discussed in this section highlight that using the proposed workflow to determine the outdoor MRT in an urban canyon is more reliable with reference to shaded areas of the canyon, whereas in sunlit areas the workflow tends to overestimate the MRT, up to 6.1 °C (at solar noon). Such discrepancy, however, is in line with the results of other studies concerning urban canyons. As an example, Rosso et al. realized an ENVI-met model with a fine mesh resolution, which led to an error by around 5 °C in the calculation of the outdoor MRT [18]. Naboni et al. used the Ladybug tools to calculate the outdoor MRT over three consecutive days [42]: the results of the simulations frequently overestimated the measured MRT by more than 5 °C, especially in the morning hours. This proves that the prediction of the outdoor MRT through urban-scale energy simulation tools is currently a complex task, which needs further investigation and the development of finer algorithms.

Possible major factors affecting the accuracy of the workflow and justifying the discrepancy, including known limitations, are discussed in depth in Section 6.

4.3 MRT and UTCI evaluation in the canyon

This section shows some examples of the outcomes offered by the workflow, such as the spatial and temporal profiles of the MRT inside the canyon and the UTCI maps. This kind of results is beneficial to provide clear insight into the outdoor thermal comfort perceived by pedestrians, and to point out critical areas within the canyon in the various moments of the day.

Unlike the simulations considered in the previous section, in this case, the weather file has not been modified by imposing the values measured during the experimental campaign. This means that the workflow fully exploits the morphing procedure operated by Dragonfly. The results commented in this section refer only to 30th August, which is representative of any sunny day in summer.

As a first example, Figure 11 shows the MRT profile through the width of the canyon, between building #2 and building #5, along the line reported in Figure 10. The very high MRT values occurring at 14:00 between point A and point C, ranging from 48 °C to 54 °C, are justified by the direct solar radiation hitting the ground and the façade of building #2, as well as any pedestrian

walking here. Point D and point E are in the shade, due to the shading effect of building #5: here, the MRT values at 14:00 lie between 34 °C and 35 °C.

Furthermore, Figure 11 suggests that the MRT at morning and in the late afternoon is almost uniform through the canyon and does not exceed 40 °C. At 10:00 all points except point E receive direct solar radiation; however, its intensity is weak and not sufficient to produce considerable overheating of the ground surface. On the other hand, at 17:00, the sun position is low and all the points are in the shade, which justifies the lower MRT values.

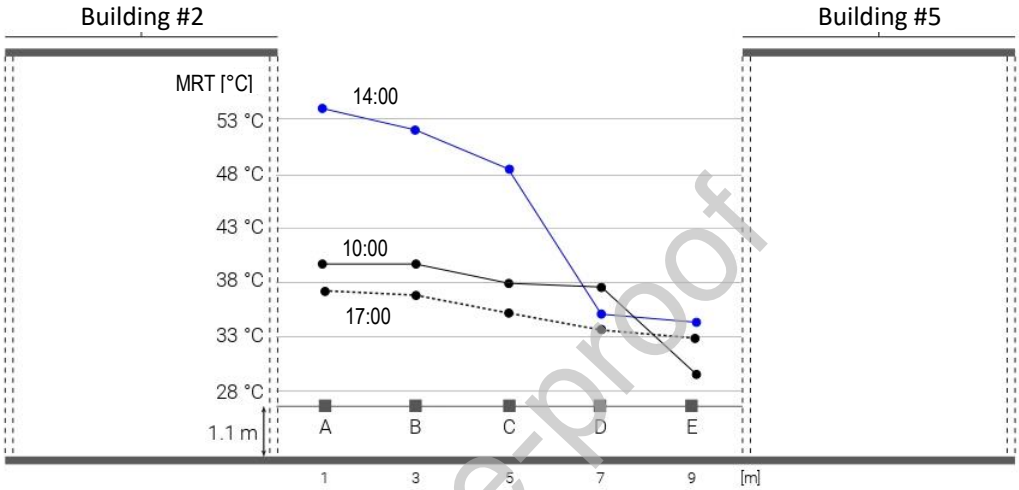

Figure 11 – MRT profiles along the central section of the canyon (30th August)

One more potential output from the proposed parametric workflow is the UTCI map. Figure 12 reports three maps, referring to three different moments of the day. The worst situation occurs at 14:00, when in a large portion of the canyon the UTCI ranges between 35 °C and 37 °C. This implies strong heat stress according to the UTCI categories (see Table 1). In the remaining areas of the canyon, and particularly in the shaded areas, the UTCI is between 30 °C and 32 °C, meaning moderate heat stress. The different values of the UTCI through the canyon are consistent with Eq. (4): this suggests that at any given time with specific values of outdoor air temperature, relative humidity and wind airspeed, a spatial variation of the MRT by 1 °C generates a UTCI variation by 0.25°C. Finally, the perceived outdoor thermal comfort is slightly better at 17:00, when the UTCI does not exceed 34 °C (Figure 12): nevertheless, this still implies strong heat stress. On the contrary, at 10:00, the UTCI is below 32 °C: this condition leads to moderate heat stress.

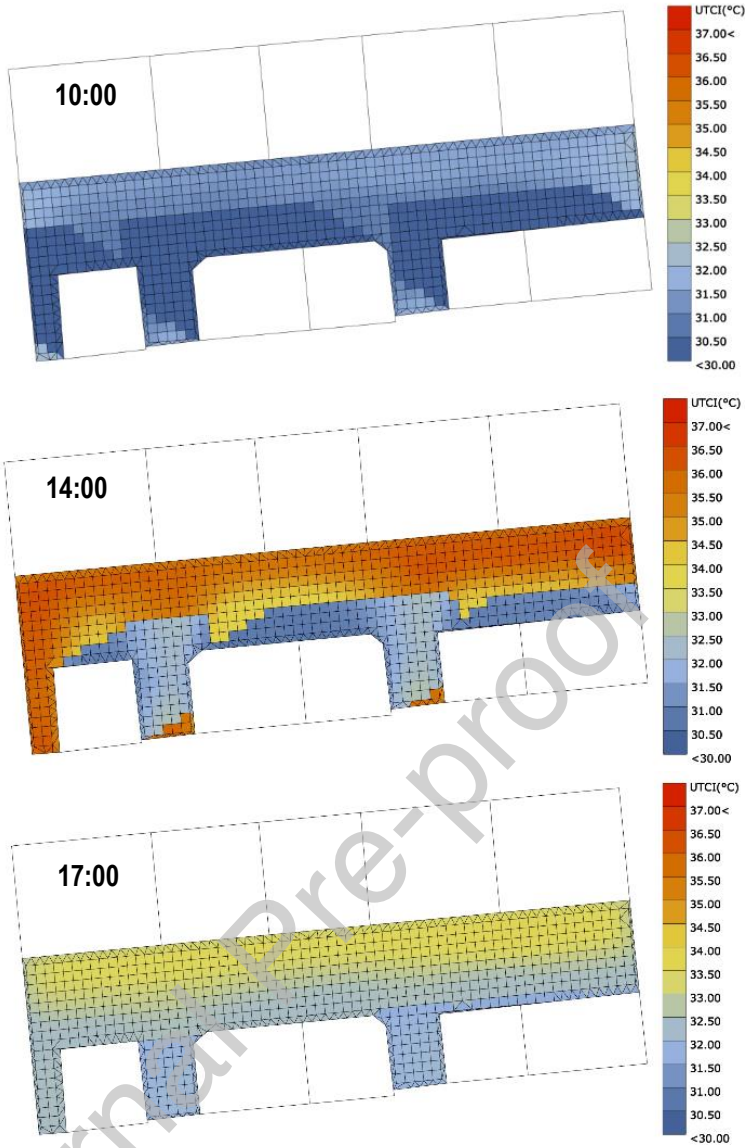

Figure 12 – UTCI maps for three different hours on 30th August

5. Effect of the surface albedo on the outdoor comfort and the building energy demand

This section discusses the results of an investigation aimed at identifying the effect of lower albedo values on the outdoor thermal comfort conditions perceived within the urban canyon, measured through the UTCI. In addition, the parametric analysis considers the energy demand for space heating and cooling of the buildings facing the canyon, calculated by the workflow as described in Section 2.4. The aims of this parametric analysis are manifold. Firstly, it is useful to check the coherence of the results both with physical common sense and with other findings already discussed in the literature, thus contributing to the identification of possible inconsistencies in the workflow. Then, it shows the ability of the workflow to describe the effect of a design parameter on both the indoor and the outdoor environment, which is one of its main strong points. This last issue is

particularly relevant when dealing with any parameter regarding the building envelope and its role of "climate giver" for the indoor and the outdoor living spaces.

This parametric analysis is performed through three additional simulations where the albedo of the facades and the ground surface is modified starting from the values adopted in the previous section, identified as "Case A" (see Table 7). In particular, in "Case B" the albedo of the buildings located along the Northern side of the canyon – with their facades facing South – is set to r = 0.4, while other surfaces keep the same albedo as in "Case A". In "Case C", this same variation of the albedo applies only to the facades of the buildings located along the Southern side. Finally, "Case D" modifies just the albedo of the ground, and proposes r = 0.05, which is the lowest possible albedo for asphalt according to the literature.

The results of this parametric analysis are shown in Table 8 and Figure 13. The time profile of the thermal load for space heating and cooling is calculated by setting an ideal thermostatic control for the indoor air temperature at 20 °C in winter and at 26 °C in summer and is then integrated over the entire season. The first value is imposed by Italian regulations in case of space heating systems, while the second value corresponds to the indoor comfort temperature for people involved in sedentary indoor activities.

The results reported in Table 8 are the mean values for all the buildings belonging to the selected portion of the urban canyon. On the other hand, the results shown in Figure 13 refer to the UTCI at 14:00 on 30th August for two different points: one is the measurement point identified in Figure 10, which was in the shade, while the second point 5 m away and is under direct sunlight.

Table 7 – Albedo values for the proposed cases ("-" means that the same value as in Case A applies)

Facade	Case A	Case B	Case C	Case D
#1	0.7	0.4	-	-
#2	0.55	0.4	-	-
#3	0.6	0.4	-	-
#4	0.6	-	0.4	-
#5	0.5	-	0.4	-
#6	0.4	-	0.4	-
Ground	0.2	-	-	0.05

Table 8 – Mean seasonal energy demand for space heating/cooling, and variation compared to Case A

		Case A	Case B	Case C	Case D
Cooling	(kWh/m^2)	20.4	21.4 + 5.0 %	20.6 + 1.0%	20.4 =
Heating	(kWh/m^2)	11.8	11.4 - 3.5 %	11.6 - 1.8 %	11.8 =
TOTAL	(kWh/m^2)	32.2	32.8 + 1.8 %	32.3 =	32.2 =

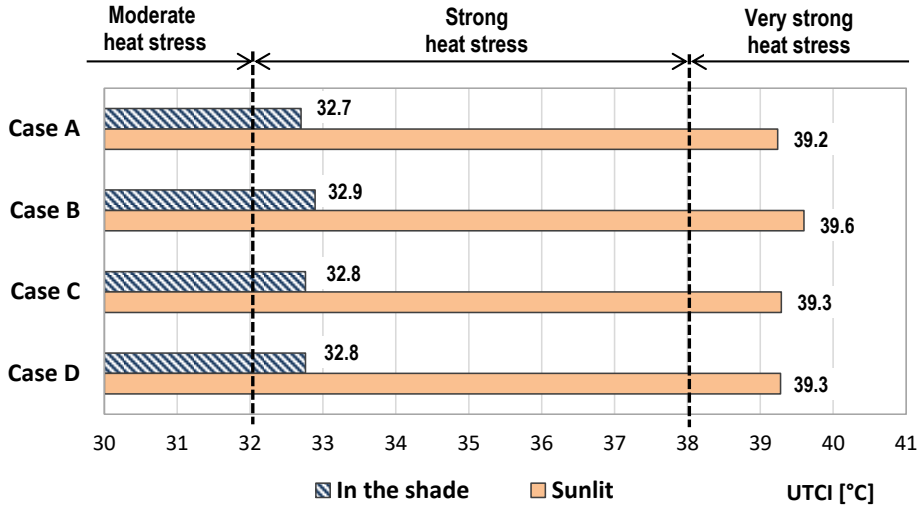

Figure 13 – Effect of the albedo on the outdoor thermal comfort

The parametric analysis suggests that a reduction in the albedo of the facades exposed to the direct beam solar radiation, as in Case B, brings about adverse effects. In particular, the UTCI perceived in a sunlit point of the canyon increases by 0.4 °C (see Figure 13), but such an effect reduces to 0.2 °C in the shade. Moreover, the mean seasonal energy demand for space cooling increases by 5 % in the summer (Table 8); on the contrary, in the winter the buildings benefit from the higher solar absorption rate, and the mean energy demand for space heating decreases by 3.5 %. On an annual basis, the total energy demand in the canyon increases by nearly 2 % if compared to Case A. Of course, the above variations would be higher if referred only to the buildings along the Northern side of the canyon: in this study, however, the attention is focused on the entire urban canyon.

On the other hand, a lower albedo for the buildings facing North, as in Case C, has almost negligible consequences. Indeed, the impact of the albedo on the thermal performance is minor for a facade hit by the diffuse solar radiation only, as in this case. Hence, the variation of the average energy demand compared to Case A is below 2 % in winter, and becomes negligible on an annual basis (Table 8). The changes induced in terms of UTCI values are negligible, too (see Figure 13).

The parametric analysis also suggests that decreasing the asphalt albedo from $r = 0.2$ to $r = 0.05$ has only minor consequences in terms of outdoor thermal comfort, as highlighted in Figure 13, where the results for Case D are very close to Case A. Actually, it is true that the higher absorption rate implies a higher ground surface temperature, hence a more intense long-wave radiant heat transfer from the ground to the pedestrians. However, this effect is offset by the lower short-wave reflection rate from the ground, which makes in this case, the UTCI values almost unchanged. Finally, the variation of the asphalt albedo does not affect the energy needs of the buildings.

6. Discussion about the limitations of the workflow

The workflow developed in this study aims at coupling the outdoor and indoor thermal fields within a unique simulation environment provided by the Ladybug Tools in the Grasshopper environment. This feature is particularly useful to assess the effectiveness of mitigations strategies in urban areas under a broad perspective. However, such a comprehensive approach needs the adoption of some simplified assumptions and algorithms in order to reduce the computational burden, thus introducing possible inaccuracies that are worthy of discussion and further refinement. This particularly applies to the appraisal of the outdoor thermal field, while the definition of the indoor thermal conditions relies on widely validated simulation engines such as EnergyPlus and OpenStudio.

More in detail, the validation exercise reported in Section 4.2 has proved that the proposed workflow works well in predicting the outdoor MRT distribution within an urban canyon under shaded conditions, with absolute differences with experimental measurements below 0.6 °C. On the other hand, significant overestimation of the MRT occurs in points exposed to direct sun (up to 6.1 °C in this study). Similar discrepancies can be observed when looking at the ground surface temperature: in this case, the simulations overestimate the value by around 4 °C in sunlit areas.

The results of the parametric analysis discussed in Section 5, regarding the variation of the albedo for the various surfaces, are consistent. However, the effect of the albedo in terms of outdoor thermal comfort is still debated in the literature. Recent studies have underlined that in some cases lighter facades can increase the outdoor Mean Radiant Temperature, due to the higher fraction of short-wave radiation reflected towards the pedestrians [15, 18]. This outcome depends on many parameters, such as the shape of the canyon, the role of the wind speed and the position of the pedestrians.

These results provide several suggestions about possible inaccuracies in the model. The first one refers to the representation of the ground surface. In fact, the Grasshopper tools need to manage it as a surface of a thermal zone in order to calculate its temperature; for this reason, a fictitious ground thermal zone was introduced in the model. However, no references are available in the literature about the definition of this ground thermal zone. In this paper, the authors reasonably defined it as an enclosure with adiabatic surfaces except for its roof, which corresponds to the street surface; the internal temperature of this fictitious zone is kept at a constant set-point temperature of 18 °C, that is to say, the default ground temperature used by EnergyPlus. The thickness of the roof is set at 50 cm, and its thermal properties correspond to weathered asphalt. Further investigations should verify possible improvements in the definition of the ground thermal zone, e.g. the role of settings like the fictitious indoor temperature, the asphalt thickness and its thermal capacity, while

also checking the appropriateness of the algorithms used to assess convective and long-wave radiant heat exchange at the ground surface [61]. Once the accuracy of the surface temperatures is verified, the calculation of the long-wave component for the MRT is reliable thanks to the ray-tracing approach adopted in the definition of the view factors.

The results discussed above also suggest an inaccuracy in predicting the amount of solar radiation hitting the grid of points at 1.1 m above the ground surface, representing possible positions of the pedestrians. This may originate from the SolarCal algorithm: indeed, the calculation of the outdoor MRT does not account for the short-wave radiation reflected from the facades, and approximates the short-wave radiation reflected from the ground, as described in Section 2.1. Actually, the SolarCal algorithm was initially developed for indoor environments, where the role of the direct solar radiation reflected by the walls is minor [45]. Hence its application to outdoor environments is questionable.

Further possible sources of inaccuracy lie in the estimation of the wind patterns and of the UHI effect. For the first aspect, the wind speed and direction are retained from the ".epw" weather file, and do not take into account the actual wind distribution within the specific urban canyon. This implies inaccuracy in the evaluation of the convective heat transfer coefficient for all surfaces in the canyon, hence in the calculation of their temperature. The most accurate way to include the modified patterns in an urban settlement would consist in running detailed yet cumbersome CFD analysis [62]. This is currently an open research field, where simplified but reliable tools for wind flow analysis have started being also developed in the Grasshopper environment. One of these tools is Eddy, a plug-in to incorporate wind and outdoor comfort analyses into sustainable architectural design, which focuses on annual ventilation analyses by employing both cylindrical and box-shaped simulation domains [63]. This could help in closing the simulation loop and allows for complete integration with the workflow.

As far as the UHI effect is concerned, the UWG model implemented in Dragonfly actually derives average geometric data and materials' properties based on a comprehensive portion of the urban texture: then, these are fed into the Urban Canopy layer model and thus estimate urban air temperature and relative humidity. The results may deviate from the microclimatic parameters actually experienced in the specific urban canyon, and are somewhat representative of a broader urban context [39]. On the one hand, they can still be undoubtedly useful to improve the accuracy in the calculation of the building thermal load if compared to the mere adoption of the rural weather file; moreover, a deviation by few degrees in the outdoor air temperature has no significant effects on the prediction of the outdoor MRT, especially in sunlit areas. On the other hand, according to Eq. (4) there is a strong correlation between UTCI and the outdoor air temperature: as an example,

an underestimation by 2 °C in the air temperature would generate an underestimation by 1.7 °C in the UTCI.

Finally, in their current version, the Ladybug tools are not able to account for the cooling effect produced by trees and other green areas through the evapotranspiration process, while it is possible to simulate their shading effect. In any case, these effects are not relevant in this study since there is no greenery in the selected urban canyon.

In the end, the workflow is an interesting tool to estimate the MRT distribution in urban canyons and the effectiveness of suitable mitigation actions through appropriate metrics such as the UTCI, while also assessing the energy implications for the operation of buildings in urban areas.

The authors are currently working on the possibility of improving the workflow, also by verifying the algorithms implemented in some components.

7. Conclusions

The paper has introduced a novel holistic workflow that can simulate the thermal interaction of buildings with the outdoor space at a district scale. The workflow is implemented in Grasshopper and relies on its freely available plug-ins Honeybee, Ladybug and Dragonfly. As a result, it allows calculating the dynamic thermal load of the buildings overlooking the canyon together with several parameters needed to assess the outdoor thermal comfort via suitable metrics such as the *Mean Radiant Temperature* (MRT) and the *Universal Thermal Climate Index* (UTCI). In the simulations, the workflow also accounts for the UHI effect through a morphing procedure that converts the available rural weather datasets into an urban weather dataset, according to the Urban Weather Generator (UWG) model.

The reliability of such a modelling approach is tested in an urban canyon located in Catania, Southern Italy, where the facades have relatively high average albedo values. In particular, the results concerning the MRT are compared to on-site measurements performed with a black globe thermometer during both sunny and shaded conditions in different summer days. The results of the validation are very encouraging when the MRT is computed for a point shaded from the direct sun: in fact, the absolute differences with the experimental measurements proved to be always below 0.6 °C. Conversely, the error recorded when considering a point that is directly hit from sunlight can be as high as 6.1 °C. This inaccuracy may lie in the way the street surface is modelled – which is actually considered as the roof surface of a fictitious "ground thermal zone" – and in the appraisal of the temperature of the other surfaces facing the canyon. In fact, multiple reflections of sun rays are not currently taken into account.

Despite this, the workflow produces consistent results when running a parametric analysis of the canyon albedo. Indeed, a lower albedo (r = 0.4) than the actual values (between 0.5 and 0.7) for the South-facing facades induces an increase by up to 0.4 °C in the UTCI perceived by pedestrians in the canyon, and higher energy needs for space cooling (+ 5% on the mean value for all buildings in the canyon). On the contrary, a lower albedo (r = 0.4) for the buildings facing North has negligible consequences in terms of outdoor thermal comfort and energy needs for heating and cooling, and similar results occur when decreasing the asphalt albedo from r = 0.2 to r = 0.05.

In comparison to other existing approaches, the workflow proposed in this paper offers greater flexibility and the complete modelling of the indoor/outdoor thermal fields on a single software platform. This makes it possible to perform a parametric investigation of the effects of different design solutions on the indoor and outdoor environment, both for new and existing buildings, of rather large spatial domains with an hourly time step.

The inaccuracy in predicting outdoor comfort conditions under sunny occurrences, as well as the integration with easy-to-use yet accurate CFD simulations within the same Grasshopper platform, will be further investigated by the authors in future research.

Nomenclature

Variables	
d	Diameter (m)
ERF	Effective Radiant Field (W m^{-2})
$\mathbf{f_{eff}}$	Effective body fraction (-)
F	View Factor (-)
$\mathbf{h_c}$	Convective heat transfer coefficient (W m^{-2} K^{-1})
$\mathbf{h_r}$	Radiant heat transfer coefficient (W m^{-2} K^{-1})
L	Horizontal infrared radiation intensity (W m^{-2})
MRT	Mean Radiant Temperature (°C)
RH	Relative Humidity (%)
T	Temperature (°C)
UTCI	Universal Thermal Climate Index (°C)
v	Wind velocity (m s^{-1})
Greek letters	
ε	Thermal emissivity (-)
σ	Stefan-Boltzmann constant (W m^{-2} K^{-4})
Subscripts	
a	air
g	globe
LW	long wave
Sky	sky

8. References

1. Andreou, E., Axarli, K. (2012). Investigation of urban canyon microclimate in traditional and contemporary environment. Experimental investigation and parametric analysis. *Renewable Energy* 43, 354-363.
2. Naboni, E., Havinga, L. (2019). Regenerative design in digital practice: a handbook for the built environment. Bozen-Bolzano: Eurac Research, 2019.
3. Bourbia, F., Boucheriba, F. (2010). Impact of street design on urban microclimate for semi arid climate (Constantine). *Renewable Energy* 35, 343–347.
4. Emmanuel, R., Johansson, E. (2006). Influence of urban morphology and sea breeze on hot humid microclimate: The case of Colombo, Sri Lanka. *Climate Research* 30(3), 189–200.
5. Achour-Younsi, S., Kharrat, F. (2016). Outdoor thermal comfort: Impact of the geometry of an urban street canyon in a Mediterranean subtropical climate – Case study Tunis, Tunisia. *Procedia - Social and Behavioral Sciences* 216, 689-700.
6. Sözen, I., Oral, G.K. (2019). Outdoor thermal comfort in urban canyon and courtyard in hot arid climate: A parametric study based on the vernacular settlement of Mardin. *Sustainable Cities and Societies* 48, 101398.
7. Rodriguez Algeciras, J.A., Gomez Consuegra, L., Matsarakis, A. (2016). Spatial-temporal study on the effects of urban street configurations on human thermal comfort in the world heritage city of Camagüey-Cuba. *Building and Environment* 101, 85-101.
8. Ali-Toudert, F., Mayer, H. (2006). Numerical study on the effects of aspect ratio and orientation of an urban street canyon on outdoor thermal comfort in hot and dry climate. *Building and Environment* 41, 94–108.
9. Ketterer, C., Matsarakis, A. (2014). Human-biometeorological assessment of heat stress reduction by replanning measures in Stuttgart, Germany. *Landscape and Urban Planning* 122, 78–88.
10. Sharmin, T., Steemers, K., Matzarakis, A. (2015). Analysis of microclimatic diversity and outdoor thermal comfort perceptions in the tropical megacity Dhaka, Bangladesh. *Building and Environment* 94, 734–750.
11. Sharmin, T., Steemers, K., Matzarakis, A. (2017). Microclimatic modelling in assessing the impact of urban geometry on urban thermal environment. *Sustainable Cities and Society* 34, 293–308.
12. Evola, G., Marletta, L., Cimino D. (2018). Weather data morphing to improve building energy modeling in an urban context. *Mathematical Modelling of Engineering Problems 5(3)*, 211–216.

13. Chokhachian, A., Perini, K. et al. (2017). How material performance of building façade affect urban microclimate. *Proceedings from Powerskin Conference*, Munich (Germany), 19 January 2017.
14. Erell, E., Pearlmutter, D. et al. (2014). Effect of high-albedo materials on pedestrian heat stress in urban street canyons. *Urban Climate 10*, 367–386.
15. Yang, J., Wang, Z.H., Kaloush K.E. (2015). Environmental impacts of reflective materials: is high albedo a 'silver bullet' for mitigating urban heat island? *Renewable and Sustainable Energy Reviews 47*, 830–843.
16. Schrijvers, P.J.C., Jonker H.J.J. et al. (2016). The effect of using a high-albedo material on the Universal Temperature Climate Index within a street canyon. *Urban Climate 17*, 284–303.
17. Laureti, F., Martinelli, L., Battisti, A. (2018). Assessment and mitigation strategies to counteract overheating in urban historical areas in Rome. *Climate* 6, 18.
18. Rosso, F., Golasi, I. et al. (2018). On the impact of innovative materials on outdoor thermal comfort of pedestrians in historical urban canyons. *Renewable Energy* 118, 825–839.
19. Battisti, A., Laureti, F., Zinzi, M., Volpicelli, G. (2018). Climate mitigation and adaptation strategies for roofs and pavements: a case study at Sapienza University campus. *Sustainability* 10, 3788.
20. Taleghani, M., Berardi, U. (2018) The effect of pavement characteristics on pedestrians' thermal comfort in Toronto. *Urban Climate* 24, 449–459.
21. Santamouris, M., Cartalis, C., Synnefa, A., Kolokotsa, D. (2015). On the impact of urban heat island and global warming on the power demand and electricity consumption of buildings – A review. *Energy and Buildings* 98, 119–124.
22. Santamouris, M. (2014). On the energy impact of urban heat island and global warming on buildings. *Energy and Buildings* 82, 100–113.
23. Steeneveld, G.J., Koopmans, S., Heusinkveld, B.G., van Hove, L.W.A., Holtslag, A.A.M. (2011). Quantifying urban heat island effects and human comfort for cities of variable size and urban morphology in the Netherlands. *Journal of Geophysical Research* 116, D20129, doi:10.1029/2011JD015988.
24. Vuckovic, M., Kiesel, K., Mahdavi, A. (2016). Toward advanced representations of the urban microclimate inbuilding performance simulation. *Sustainable Cities and Society* 27, 356–366.
25. Santamouris, M. (2020). Recent progress on urban overheating and heat island research. integrated assessment of the energy, environmental, vulnerability and health impact synergies with the global climate change. *Energy and Buildings 207*, 109482.
26. Palme, M., Inostroza, L., Villacreses, G., Lobato-Cordero, A., Carrasco, C. (2017). From urban climate to energy consumption. Enhancing building performance simulation by including the urban heat island effect. *Energy and Buildings* 145, 107–120.

27. Liu, Y., Stouffs, R., Tablada, A., Hien Wong, N., Zhan, J. (2017). Comparing micro-scale weather data to building energy consumption in Singapore. *Energy and Buildings* 152, 776–791.
28. Pyrgou, A., Castaldo, V.L., Pisello, A.L., Cotana, F., Santamouris, M. (2017). On the effect of summer heatwaves and urban overheating on building thermal-energy performance in central Italy. *Sustainable Cities and Society* 28, 187–200.
29. Pisello, A.L., Pignatta, G., Castaldo, V.L., Cotana, F. (2015). The impact of local microclimate boundary conditions on building energy performance. *Sustainability* 7, 9207–9230. doi:10.3390/su7079207.
30. Naboni, E., Meloni, M., Coccolo, S., Kaempf, J., Scartezzini, J-L. (2017). An overview of simulation tools for predicting the mean radiant temperature in an outdoor space. *Energy Procedia 122*, 1111-1116.
31. Noro, M., Lazzarin, R. (2015). Urban heat island in Padua, Italy: Simulation analysis and mitigation strategies. *Urban Climate* 14, 187–196.
32. Karakounos, I., Dimoudi, A., Zora, S. (2018). The influence of bioclimatic urban redevelopment on outdoor thermal comfort. *Energy and Buildings* 158, 1266–1274.
33. Tsitoura, M., Michailidou, M., Tsoutsos, T. (2016). Achieving sustainability through the management of microclimateparameters in Mediterranean urban environments during summer. *Sustainable Cities and Society* 26, 48–64.
34. Fabbri, K., Costanzo, V. (2020). Drone-assisted infrared thermography for calibration of outdoor microclimate simulation models. *Sustainable Cities and Society* 52, 101855.
35. Castaldo, V., Pisello, A.L., Piselli, C., Fabiani, C., Cotana, F., Santamouris, M. (2018). How outdoor microclimate mitigation affects building thermal-energy performance: A new design-stage method for energy saving in residential near-zero energy settlements in Italy. *Renewable Energy* 127, 920-935.
36. Fang, Y., Cho, S. (2019). Design optimization of building geometry and fenestration for daylighting and energy performance. *Solar Energy* 191, 7-18.
37. Lavin, C., Fiorito, F. (2017). Optimization of an external perforated screen for improved daylighting and thermal performance of an office space. *Procedia Engineering* 180, 571-581.
38. Elwy, I., Yasser, I., Fahmy, M., Mahdy, M. (2018). Outdoor microclimatic validation for hybrid simulation workflow in hot arid climates against ENVI-met and field measurements. Energy Procedia 153, 29–34.
39. Salvati, A., Coch Roura, H., Cecere, C. (2017). Assessing the urban heat island and its energy impact on residential buildings in Mediterranean climate: Barcelona case study. *Energy and Buildings* 146, 38–54.

40. Bajsanski, I.V., Milosevic, D.D., Savic, S.M. (2015). Evaluation and improvement of outdoor thermal comfort in urban areas on extreme temperature days: Application of automatic algorithms. Building and Environment 94, 632-643.
41. Perini, K., Chokhachian, A., Dong, S., Auer, T. (2017). Modelling and simulating urban outdoor comfort: Coupling ENVI-Met and TRNSYS by Grasshopper. *Energy and Buildings* 152, 373-384.
42. Naboni, E., Danzo, E., Ofria, L.A., (2019). Parametric workflow to conceive facades as indoor and outdoor climate givers. *Proceedings from SimAUD 2019: Symposium on Simulation For Architecture And Urban Design*. Atlanta (USA), 7-10 April 2019.
43. Bueno, B., Norford, L., Hidalgo, J., Pigeon, G. (2013). The Urban Weather Generator. Journal of Building Performance Simulation 6:4, 269-281, doi: 10.1080/19401493.2012.718797.
44. Bueno, B., Roth, M., Norford, L., Li, R. (2014). Computationally efficient prediction of canopy level urban air temperature at the neighbourhood scale. Urban Climate 9, 35–53.
45. Arens, E., Hoyt, T. et al. (2015). Modeling the comfort effects of short-wave solar radiation indoors. *Building and Environment 88*, 3-9.
46. Fanger P.O. (1970). Thermal comfort. New York: McGraw-Hill Inc.
47. Mackey, C., Galanos, T., Norford, L., Roudsari, M. (2017). Wind, sun, surface temperature and heat island: critical variables for high-resolution outdoor thermal comfort. *Proceedings from BS2017: Building Simulation Conference*. San Francisco (USA), 7-9 August 2017.
48. ASHRAE (2013). ANSI/ASHRAE Standard 55-2013: Thermal Environmental Conditions for Human Occupancy. American Society of Heating, Refrigerating and Air-Conditioning Engineers (ASHRAE).
49. Błażejczyk, K., Jendritzky, G. et al. (2013). An introduction to the Universal Thermal Climate Index (UTCI). *Geographia Polonica 86 (1)*, 5-10.
50. Błażejczyk, K. (2011). Mapping of UTCI in local scale (the case of Warsaw). *Prace i Studia Geograficzne 47*, 275–283.
51. Salvati, A., Monti, P., Coch Roura, H., Cecere, C. (2019). Climatic performance of urban texture: analysis tools for a Mediterranean urban context. *Energy and Buildings 185*, 162-179.
52. Gimenez, L., Hippolyte, J.L., Robert, S., Suard, F., Zreik, K. (2015). Review: Reconstruction of 3D building information models from 2D scanned plans. *Journal of Building Engineering* 2, 24–35. https://doi.org/10.1016/j.jobe.2015.04.002.
53. DOE, US Department of Energy, www.energycodes.gov/development/residential/iecc_models (last accessed November 2019).
54. SIAS, Sicilian Agrometeorological Informative Systems, www.sias.regione.sicilia.it/home.htm (last accessed November 2019)
55. ASHRAE (2001). ASHRAE Handbook - Fundamentals. GA, USA: Atlanta.

56. Kantor, N., Unger, J. (2011). The most problematic variable in the course of human-biometeorological comfort assessment: the mean radiant temperature. *Central European Journal of Geosciences 3*, 90-100.
57. Chen, Y.C., Lin, T.P., Matzarakis, A. (2014). Comparison of mean radiant temperature from field experiment and modelling: a case study in Freiburg, Germany. *Theor. Appl. Climatol*. 118 535–551. doi:10.1007/s00704-013-1081-z.
58. Thorsson, S., Lindberg, F., Eliasson, I., Holmer, B. (2007). Different methods for estimating the mean radiant temperature in an outdoor urban setting, *International Journal of Climatology* 27, 1983–1993.
59. Marino, C., Nucara, A., Pietrafesa, M., Costanzo S. (2018). Outdoor mean radiant temperature estimation: is the black-globe thermometer method a feasible course of action? *Proceedings from IEEE EEEIC18: 18th Intern. Conf. on Environment and Electrical Engin*. Palermo (Italy), 12-15 June 2018.
60. Elements tool User guide, Rocky Mountain Institute, https://bigladdersoftware.com/projects/elements/docs/user-guide/ (last accessed December 2019).
61. Costanzo, V., Evola, G., Marletta, L., Gagliano, A. (2014). Proper evaluation of the external convective heat transfer for the thermal analysis of cool roofs. *Energy and Buildings* 77, 467–477.
62. Toparlar, Y., Blocken, B., Maiheu, B., Van Heijst, G.J.F. (2017). A review on the CFD analysis of urban microclimate, *Renewable and Sustainable Energy Reviews* 80, 1613-1640.
63. Dogan, T., Kastner, P. Streamlined CFD simulation framework to generate wind-pressure coefficients on building facades for airflow network simulations. *Proceedings from the 7th International Building Physics Conference*, Syracuse (USA), 23 July 2018.

Author	**Contribution**
Gianpiero Evola	Conceptualization, Methodology, Formal analysis, Investigation, Writing Original draft + Review & Editing, Project administration
Vincenzo Costanzo	Formal analysis, Investigation, Writing Original draft + Review & Editing
Cristina Magrì	Software, Investigation

Giuseppe Margani	Conceptualization, Methodology, Writing - Review & Editing
Luigi Marletta	Writing - Review & Editing, Resources, Supervision
Emanuele Naboni	Conceptualization, Methodology, Writing - Review & Editing